

## Crystal structure, surface structure and chemical analysis of $\text{BaFe}_{10.8}\text{In}_{1.2}\text{O}_{19}$ compound

G.Sh. Ayyubova<sup>1\*</sup>, S.H. Jabarov<sup>2</sup>

<sup>1</sup>Scientific Research Institute of Aerospace Informatics, Azerbaijan National Aerospace Agency, Baku, AZ-1106, Azerbaijan

<sup>2</sup>Azerbaijan State Pedagogical University, Baku AZ1072, Azerbaijan  
e-mail: [gulerayyubova90@gmail.com](mailto:gulerayyubova90@gmail.com)

---

### Abstract

In this work, the compound  $\text{BaFe}_{10.8}\text{In}_{1.2}\text{O}_{19}$  was synthesized and analyzed using a Scanning Electron Microscope (SEM). The synthesis process was carried out according to the standard procedure. The crystal structure, surface structure and chemical analysis of the obtained polycrystals have been investigated. It was found that the crystal structure of the  $\text{BaFe}_{10.8}\text{In}_{1.2}\text{O}_{19}$  compound corresponds to a highly symmetric hexagonal system. It was found that the size of crystallites in  $\text{BaFe}_{10.8}\text{In}_{1.2}\text{O}_{19}$  is in the range  $d \sim 1\text{-}10 \mu\text{m}$ . Chemical analysis showed that this compound consists of 40.9% - Fe, 38.7% - O, 11.1% - Ba and 8.2% - In atoms.

**Keywords:** hexaferrite, SEM, multiferroic, crystal structure, surface structure

---

Received: 10 december 2021

Accepted: 20 december 2021

Published: 27 december 2021

---

### 1. Introduction

The study of compounds with magnetic properties is one of the topical problems in condensed matter physics. It is known that some materials have both ferroelectric and ferromagnetic properties. Such compounds have more interesting physical properties. Barium hexaferrite and its solid solutions are considered to be such compounds. Determining the relationship between physical properties and structure of materials is very important when studying other physical properties of these components [1-3].

$\text{BaFe}_{12}\text{O}_{19}$ , which has a hexagonal crystal structure, is one of the most studied multiferroics in recent years. Barium hexaferrite is a material with ferrimagnetic properties under normal conditions and at room temperature. It was found that the ferrimagnetic-paramagnetic phase transition in this compound occurs at a temperature  $T_C \approx 750 \text{ K}$ . Previous structural studies have shown that when  $\text{Fe}^{3+}$  ions are replaced by  $\text{Ga}^{3+}$ ,  $\text{Al}^{3+}$ ,  $\text{Sc}^{3+}$  ions in barium hexaferrite, changes in the crystal structure of the compounds are observed [4-6]. An increase in the concentration of diamagnetic ions leads to a partial violation of the long-range magnetic order, thereby weakening the magnetic properties. Hexaferrites and composite materials based on them are widely used in various fields as materials that absorb electromagnetic radiation. Consequently, by preserving the magnetic properties, replacing Fe

---

atoms with In changes the electronic configuration of these materials, making them important materials for electronics and spintronics.

It is known that the crystallite size also affects other properties of the compound. Therefore, it is important to study the size effects of each research object. In this work, the crystal structure, surface structure, and chemical analysis of the  $\text{BaFe}_{10.8}\text{In}_{1.2}\text{O}_{19}$  compound were carried out. The studies were performed at room temperature and under normal conditions by XRD and SEM.

## 2. Experiments

### 2.1. Synthesis.

Investigated  $\text{BaFe}_{10.8}\text{In}_{1.2}\text{O}_{19}$  samples were obtained from high purity  $\text{Fe}_2\text{O}_3$  and  $\text{In}_2\text{O}_3$  oxides and carbonate  $\text{BaCO}_3$  by conventional solid reaction method using ‘two-steps’ topotactic reactions. At first the oxides and carbonate were mixed with design ratio. Then the pre-firing was performed at  $1200\text{ }^\circ\text{C}$  in air during 6 h. Final synthesis was carried out at  $1300\text{ }^\circ\text{C}$  in air during 6 h. After synthesis the samples were slowly cooled ( $100\text{ }^\circ\text{C h}^{-1}$ ).

### 2.2. XRD analysis.

The X-ray diffraction measurement was performed using a Bruker D8 Advance powder diffractometer with the following parameters: 40 kV, 40 mA, Cu  $K\alpha$  radiation ( $\lambda = 1.5406\text{ \AA}$ ). The X-ray diffraction data were treated using the FullProf program.

### 2.3. SEM (Scanning Electron Microscope) analysis.

Surface morphology and chemical analysis of  $\text{BaFe}_{10.8}\text{In}_{1.2}\text{O}_{19}$  were performed on SEM (Scanning Electron Microscope, ZEISS, SIGMA VP). In a Scanning Electron Microscope, a tungsten element enclosed in a zirconium ring is used as an electronic source. The operating mode for the voltage during the thermal emission process based on the Schott effect is  $0.05\text{ V}$  -  $30\text{ keV}$ , the operating distance between the beam source and the sample is assumed to be  $\leq 10\text{ mm}$ . Samples are prepared in specially selected laboratory conditions.

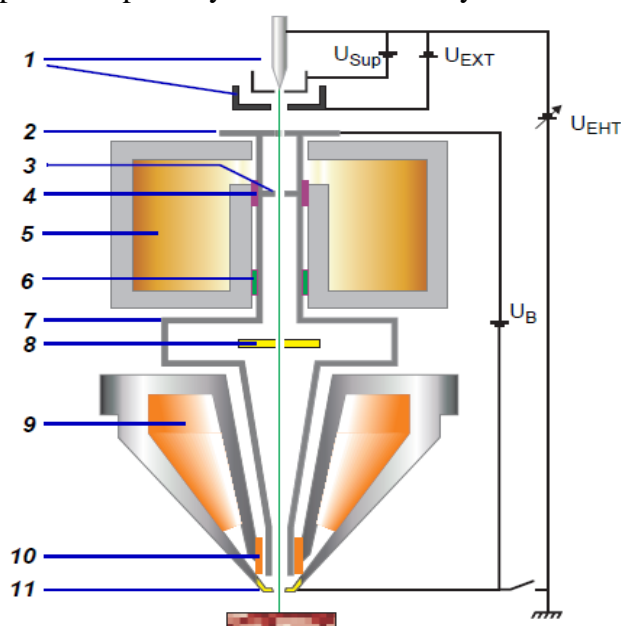


**Figure 1.** Schematic description of electron optics in Scanning Electron Microscopy: 1. Schottky field emission, 2. Anode, 3. Multichannel pores, 4. Grouping system, 5. Lens, 6. Stigmator, 7. Linear channel, 8. Detector, 9. Electromagnetic lenses, 10. Scanning camera, 11. Cover.

The carbon is pulled into trays and placed in silver slots. After placing the samples in the chamber, molecular pumps create a vacuum of  $10^{-7}$  Mbar. The main purpose of creating a high vacuum is to increase the free path of electrons and reduce the likelihood of elastic or inelastic collisions. In this case, the energy transferred to the accelerated electrons is transferred directly to the interaction of the sample atoms, which leads to a decrease in the error.

Along with the experimental part, of greater interest is the theoretical part or optics of the processes occurring in electron optics under a microscope. A schematic sequence of processes in SEM is shown in detail in Figure 3. Under the action of thermal emission, electrons emitted from the tungsten element are directed by an electrostatic field. Accelerated electrons in a potential field are accelerated up to 30 kV and interact with the sample.

### 3. Results and discussion

#### 3.1. Structural analysis.

The crystal structure of  $\text{BaFe}_{10.8}\text{In}_{1.2}\text{O}_{19}$  was studied by X-ray diffraction. The X-ray diffraction spectrum obtained under normal conditions and at room temperature is shown in Figure 2.

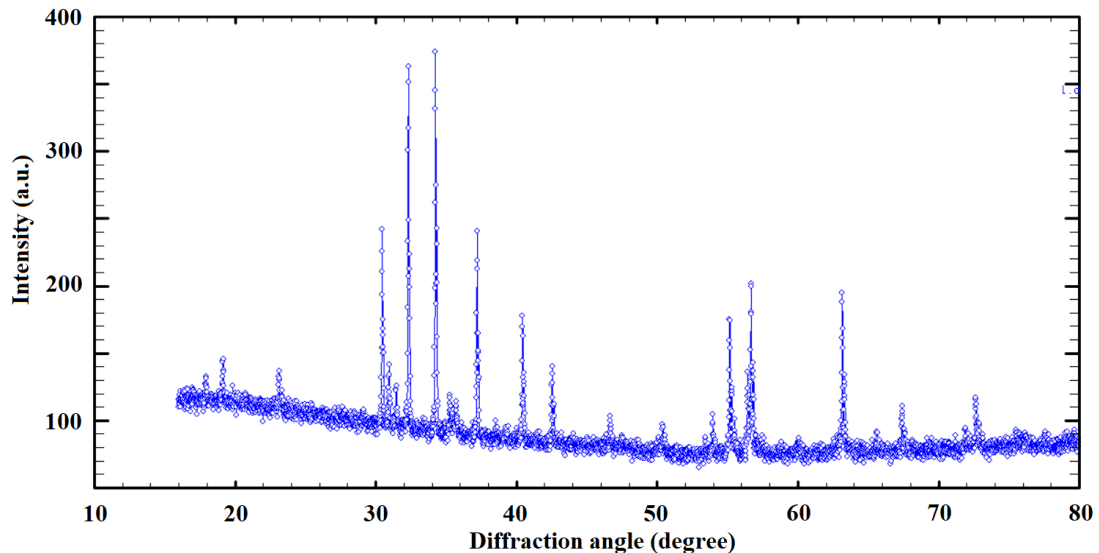


**Figure 2.** X-ray diffraction spectrum of the compound  $\text{Fe}_{10.8}\text{In}_{1.2}\text{O}_{19}$ .

As a result of the analysis of the X-ray diffraction spectrum obtained in the range of diffraction angles  $15^\circ \leq 2\theta \leq 80^\circ$ , it was determined that the crystal structure of the  $\text{BaFe}_{10.8}\text{In}_{1.2}\text{O}_{19}$  compound corresponds to the hexagonal symmetry of the space group  $P6_3/mmc$ . It is known that the crystal structure of barium hexaferrite also corresponds to the hexagonal symmetry of the space group  $P6_3/mmc$  [7-9]. As can be seen, no significant changes in the crystal structure are observed with the substitution of  $\text{Fe} \rightarrow \text{In}$  up to a concentration of  $x = 1.2$ .

#### 3.2. Surface structure.

The surface structure of  $\text{BaFe}_{10.8}\text{In}_{1.2}\text{O}_{19}$  was studied using a scanning electron microscope. A description of the surface structure is shown in Figure 3.

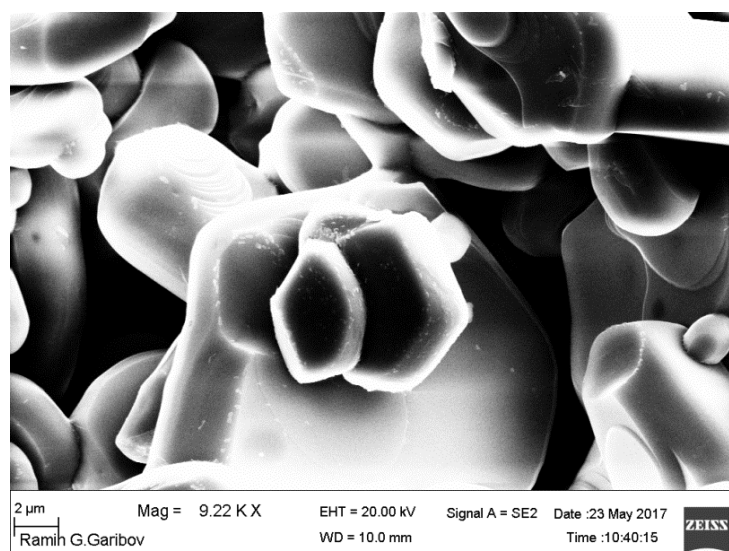


**Figure 3.** The surface structure of  $\text{Fe}_{10.8}\text{In}_{1.2}\text{O}_{19}$ , obtained with a Scanning Electron Microscope.

As can be seen from Figure 3, the crystallites of the powder sample are of different sizes. The sizes of the smallest crystallites are  $d \sim 1 \mu\text{m}$ , and the sizes of the largest crystallites are  $d \sim 26 \mu\text{m}$ . From the morphology of the crystallites, it is clear that the sample was synthesized with high quality. The object of the study was not in the form of solid solutions ( $\text{BaFe}_{1.2}\text{O}_{19}$ – $\text{BaIn}_{12}\text{O}_{19}$ ), but was synthesized in a single-phase state -  $\text{BaFe}_{10.8}\text{In}_{1.2}\text{O}_{19}$ .

### 3.3. Chemical analysis.

The chemical composition of  $\text{BaFe}_{10.8}\text{In}_{1.2}\text{O}_{19}$  was also studied during SEM analysis. The chemical analysis spectrum is shown in Figure 4.

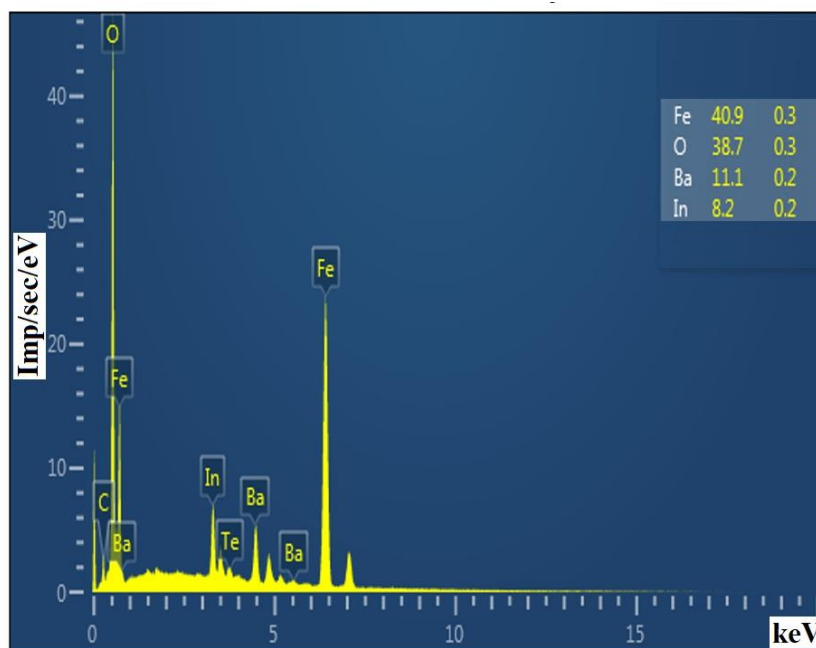


**Figure 4.** Spectrum of analysis of the chemical composition of the  $\text{BaFe}_{10.8}\text{In}_{1.2}\text{O}_{19}$  compound.

As a result of the analysis of the composition, it was determined that  $\text{BaFe}_{10.8}\text{In}_{1.2}\text{O}_{19}$  consists of 40.9% - Fe, 38.7% - O, 11.1% - Ba, and 8.2% - In. As you can see,

the substance was synthesized with a fairly high purity. A sample was synthesized with a purity of 99.9%. In the composition, very small amounts of 0.1% of other elements were obtained, which were not observed in the X-ray diffraction spectrum.

#### 4. Conclusion

The crystal structure and morphology of the  $\text{BaFe}_{10.8}\text{In}_{1.2}\text{O}_{19}$  compound were studied by X-ray diffraction and SEM. Chemical analysis of the samples was carried out. The synthesized compound was found to be synthesized with a high purity of 99.9%. The crystal structure of the obtained compound is hexagonally symmetric with the space group  $P63/mmc$  in accordance with the structures of barium hexaferrite and its solid solutions. When studying a powder sample by SEM, it was determined that the size of the smallest crystallites is  $d \sim 1 \mu\text{m}$ , and the size of the largest crystallites is  $d \sim 26 \mu\text{m}$ .

#### References

1. S.H. Jabarov, N.T. Dang, S.E. Kichanov, D.P. Kozlenko, L.S. Dubrovinsky, J.G. Park, S. Lee, A.I. Mammadov, R.Z. Mehdiyeva, B.N. Savenko, N.X. Nghia, L.H. Khiem, N.T.T. Lieu, L.T.P. Thao, *Materials Research Express* **6**(8) (2019) 086110.
2. N.T. Dang, D.P. Kozlenko, N. Tran, B.W. Lee, T.L. Phan, R.P. Madhogaria, V. Kalappattil, D.S. Yang, S.E. Kichanov, E.V. Lukin, B.N. Savenko, P. Czarnecki, T.A. Tran, V.L. Vo, L.T.P. Thao, D.T. Khan, N.Q. Tuan, S.H. Jabarov, M.H. Phan, *Journal of Alloys and Compounds* **808** (2019) 151760.
3. D.P. Kozlenko, N.T. Dang, N.O. Golosova, S.E. Kichanov, E.V. Lukin, P.J.L. Kelley, E.M. Clements, K.V. Glazyrin, S.H. Jabarov, T.L. Phan, B.N. Savenko, H. Srikanth, M.H. Phan, *Physical Review B* **98**(13) (2018) 13443.
4. A.I. Mammadov, N.T. Dang, R.Z. Mehdiyeva, A.V. Trukhanov, S.G. Asadullayeva, S.V. Trukhanov, R.E. Huseynov, S.H. Jabarov, *Modern Physics Letters B*, **34**(35) (2020) 2050411.
5. A.I. Mammadov, N.T. Dang, R.Z. Mehdiyeva, A.V. Trukhanov, R.E. Huseynov, S.V. Trukhanov, S.H. Jabarov, *Modern Physics Letters B* **34**(33) (2020) 2050381.
6. F.G. Agayev, S.H. Jabarov, G.Sh. Ayyubova, A.V. Trukhanov, S.V. Trukhanov, M.N. Mirzayev, T.G. Naghiyev, N.T. Dang, *Journal of Superconductivity and Novel Magnetism* **33** (2020) 2867-2873.
7. F.G. Agayev, S.H. Jabarov, G.Sh. Ayyubova, M.N. Mirzayev, S.V. Trukhanov, E.L. Trukhanova, M.A. Darwish, S.V. Podgornaya, D.A. Vinnik, T.P. Hoang, N.T. Dang, A.V. Trukhanov, *Physica B: Condensed Matter* **580** (2020) 411772.
8. R.E. Huseynov, A.I. Mammadov, R.Z. Mehdiyeva, A.V. Trukhanov, S.V. Trukhanov, V.A. Turchenko, T.P. Hoang, N.T. Dang, S.H. Jabarov, *Journal of the Korean Physical Society* **74**(6) (2019) 584-588.
9. S.G. Dzhabarov, A.V. Trukhanov, S.V. Trukhanov, V.A. Turchenko, V.V. Oleinik, E.S. Yakovenko, L.Yu. Matsui, L.L. Vovchenko, V.L. Launets, S. Kazakevich, *Physics of the Solid State* **58**(9) (2016) 1792-1797.